Int J Thermophys (2014) 35:693–711
DOI 10.1007/s10765-014-1607-3

Thermal Influence on Long-Distance Optical Measurement of Suspension Bridge Displacement

Luís Lages Martins · José Manuel Nunes Vicente Rebordão · Álvaro Silva Ribeiro

Received: 31 July 2013 / Accepted: 21 April 2014 / Published online: 17 May 2014

Abstract This paper discusses the thermal influence on long-distance and noncontact measurement of suspension bridge three-dimensional displacement by the use of an optical system composed of a digital camera, infrared active targets, and computational support. In this type of measurement method, the optical propagation path of light through the air can range from 250 m up to 750 m, making its measurement accuracy strongly dependent on atmospheric refraction and turbulence, phenomena that are linked to the vertical temperature gradient between the camera and targets. In addition, the adopted measurement geometrical configuration can lead to a height difference between these two elements (camera and targets) above 50 m. The paper describes the experimental setup and procedure followed for the determination of local temperature vertical gradients in the 25th of April Bridge in Lisbon (Portugal), where an optical measurement system was applied. The obtained thermal measurements are presented and applied in the evaluation of the systematic refraction vertical deviation, based on appropriate mathematical models mentioned in the paper, and for the identification of stable or unstable observation thermal conditions related to turbulence.

Keywords Displacement · Optical system · Suspension bridge · Temperature

L. Lages Martins (✉) · Á. Silva Ribeiro
Scientific Instrumentation Center, National Laboratory for Civil Engineering, Lisbon, Portugal
e-mail: lfmartins@lnec.pt

Á. Silva Ribeiro
e-mail: asribeiro@lnec.pt

J. M. Nunes Vicente Rebordão
Laboratory of Optics, Lasers and Systems, Faculty of Sciences, University of Lisbon, Lisbon, Portugal
e-mail: jmrebordao@fc.ul.pt

1 Introduction

Structural observation of bridges is necessary to ensure safe mobility of persons and goods in transport networks. Spatial and temporal measurement of relevant quantities supports safety assessment of the bridge structural condition based on the established design requirements and historical behavior. In the case of long-span suspension bridges, the complexity of three-dimensional observation becomes a challenging task considering that conventional instrumentation approaches do not provide fully appropriate solutions, namely, hydrostatic leveling and geodesic observation, due to the bridge's dynamic behavior, and displacement transducers, requiring reference points which are impossible to obtain in certain measurement regions of interest such as the bridge's central section in its main span.

To overcome known constraints, research has been developed toward the use of noncontact measurement systems, aiming to comply with the observational requirements. Optical measurement systems composed of digital cameras and active targets, combined with digital image processing techniques,[1] have become one of the most promising solutions for long-distance and noninvasive three-dimensional displacement measurements, allowing real-time and long-term observation and being able to measure large dynamic structural displacements which, in large suspension bridges, can be larger than 1 m in the vertical direction. However, the accuracy of this measurement method applied in such environmental conditions (usually over a river) strongly depends upon atmospheric turbulence and refraction, phenomena that are, in principle, linked to temperature and water-vapor gradients found along the optical propagation trajectory of light through the air.

The role of temperature monitoring becomes, therefore, critical to study the effects due to these phenomena on the optical measurement of suspension bridge displacement and to decide if corrections are needed. A knowledge of the temperature vertical gradients near cameras and targets can increase the accuracy of the vertical refractive-index mathematical model, allowing the evaluation of systematic refraction deviations of the observed target's vertical position and to identify stable or unstable thermal conditions related to turbulence

This paper describes the mathematical models which establish the relation between the temperature effects, refraction, and turbulence phenomena and also the experimental apparatus and the measurement procedure developed for the determination of the local temperature vertical gradients in the 25th of April Bridge in Lisbon (Portugal). The measurements obtained are presented and estimates are used as input data to the mathematical models described in order to draw conclusions about the direct influence of thermal conditions on turbulence and refraction and, through these, its effect on the optical measurement of the suspension bridge displacement.

[1] In the applied optical approach, the digital camera is rigidly installed in the bridge's central section of its main span, orientated toward the tower foundation where a set of four active targets with known coordinates is installed. Changes in the camera's projection center position are considered representative of the bridge's displacement, being determined by the knowledge of the camera's intrinsic parameters and targets image and world coordinates by a nonlinear optimization procedure.

2 Temperature Effects on Turbulence and Refraction Phenomena

2.1 Contribution of Thermal Effects to Atmospheric Refraction

To perform the long-distance optical measurement of suspension bridge displacement, active targets generate near-infrared light (875 nm wavelength) that is being captured by an observation camera. The light propagation is affected by the atmospheric non-homogeneity and by the different environmental conditions, namely, the air temperature which can change significantly, especially in the vertical direction. This effect creates a non-null vertical refractive-index gradient, thus justifying a nonlinear trajectory of light, as represented in Fig. 1.

In this case, the vertical target position captured by the camera corresponds to an apparent or virtual position, different from its real vertical position by an angle δ designated as the vertical refraction angle, leading to a systematic deviation of the target's vertical position used for the determination of the bridge's three-dimensional displacement.

In an operational perspective, the application of Fermat's principle [1] to this observational problem states that, the light trajectory between the target and the camera corresponds to the trajectory which minimizes the light propagation time, Δt, expressed by

$$\Delta t = \frac{1}{c} \int_{\text{target}}^{\text{camera}} n\,(s)\ \mathrm{d}s, \tag{1}$$

where ds is the infinitesimal light displacement in its trajectory, n corresponds to the refractive index which changes along the light trajectory s, and c is the speed of light in vacuum. This variational problem can be written as

$$\delta \int_{\text{target}}^{\text{camera}} n\,(s)\ \mathrm{d}s = 0, \tag{2}$$

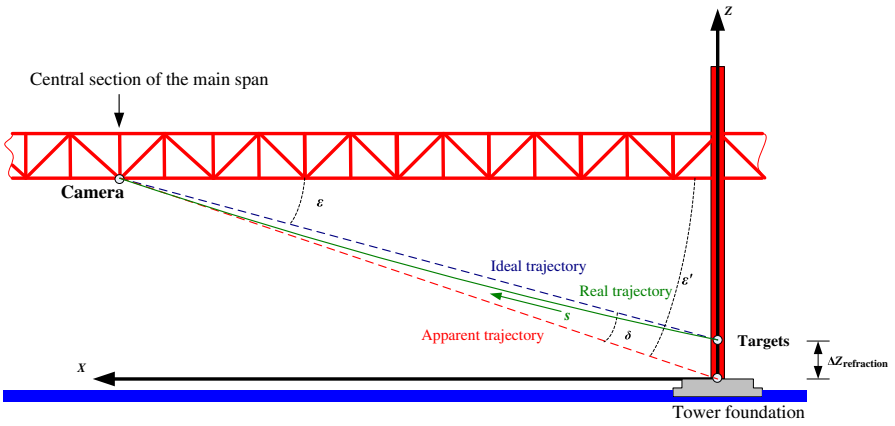

Fig. 1 Vertical refraction in long-distance bridge observation by an optical system

and its solution (similar to the Euler–Lagrange equations in classical mechanics) is given by

$$\frac{\mathrm{d}}{\mathrm{d}s}\left(n\frac{\mathrm{d}\vec{r}}{\mathrm{d}s}\right)=\nabla n, \tag{3}$$

where $\vec{r}$ is the parametric representation of the light trajectory and ∇n is the refractive-index gradient. The differential Eq. 3 has an analytical solution [1] for a constant refractive-index gradient between the targets and the camera:

$$n\,(Z)=n_0+\alpha Z, \tag{4}$$

where α is the magnitude of the vertical index gradient and n_0 is the refractive index near the light source (the active target in the studied case) positioned at Z_0. If this assumption holds, the trajectory is described by

$$X=\frac{n_0\cos(\varepsilon)}{\alpha}\ln\left(2cZ+b+2\alpha\sqrt{A+bZ+cZ^2}\right)\Big|_{Z_0}^{Z}, \tag{5}$$

where ε is the elevation angle of the ideal light trajectory relative to the X-axis (see Fig. 1) and $A=n_0^2\sin^2(\varepsilon)$, $b=2\alpha n_0$, and $c=\alpha^2$. Based on the above expression, the elevation angle of the apparent light trajectory, ε', can be obtained by

$$\varepsilon'=\arctan\left(\frac{\mathrm{d}Z}{\mathrm{d}X}\bigg|_0\right), \tag{6}$$

using a numerical method for the calculation of the derivative in the initial trajectory region close to the light source. Therefore, the vertical refraction angle, δ, becomes

$$\delta=\varepsilon-\varepsilon'. \tag{7}$$

When the nonlinearity effects related to the vertical thermal gradient are considered significant, an alternative geodesic approach [2] can be used to account for these effects on the vertical refraction angle.

Again, the vertical refraction angle can be derived from the differential Eq. 3 related to the light trajectory, based on its decomposition and relationship with the tangent and principal normal components. By assuming an isotropic medium in the transverse direction (Y-axis) and taking into account the reduced magnitude of the vertical refraction angle, the light trajectory curvature, k, can be related to the vertical index gradient by

$$k=-\frac{\cos(\varepsilon)}{n}\frac{\mathrm{d}n}{\mathrm{d}Z}. \tag{8}$$

Since the vertical refraction angle near the targets is related to the trajectory curvature by

$$\delta=\frac{1}{S}\int_0^S k\,(S-s)\,\mathrm{d}s, \tag{9}$$

where S is the curvilinear length of the light trajectory from the targets to the camera, it can also be written as

$$\delta = -\frac{\cos(\varepsilon)}{S}\int_0^S \frac{1}{n}\frac{\mathrm{d}n}{\mathrm{d}Z}(S-s)\,\mathrm{d}s. \tag{10}$$

This expression shows that the knowledge of the refractive index and its vertical gradient along the light trajectory is the key influence to the accuracy of the vertical refraction angle. It also reflects that their contribution is quite relevant in the trajectory initial path (close to the targets) and tends to decrease until it becomes null in the trajectory final path (near the camera). This behavior of measurement should be expected considering that the thermal vertical gradient can have strong nonlinearity near the bridge foundation top surface (mainly due to incident solar radiation) and tends to become linear with increasing altitude [3].

The quantification of the vertical refraction angle by Eq. 10 implies performing numerical integration using, for example, the Simpson method, and obtaining

$$\delta = -\frac{S\cos(\varepsilon)}{6}\left[\left(\frac{1}{n}\right)_{\mathrm{t}}\left(\frac{\mathrm{d}n}{\mathrm{d}Z}\right)_{\mathrm{t}} + 2\left(\frac{1}{n}\right)_{\mathrm{m}}\left(\frac{\mathrm{d}n}{\mathrm{d}Z}\right)_{\mathrm{m}}\right], \tag{11}$$

where the t and m labels refer, respectively, to the calculation of the refractive index and vertical gradient near the target and at a middle height between targets and camera.

In this study, the calculation of the refractive index of humid air is supported by Ciddor's refractivity model [4], being valid for near-infrared radiation emitted by the active targets (875 nm wavelength). The expression for the refractivity of moist air corresponds to

$$10^8(n-1) = 10^8\left[\left(\frac{\rho_{\mathrm{a}}}{\rho_{\mathrm{axs}}}\right)(n_{\mathrm{axs}}-1) + \left(\frac{\rho_{\mathrm{w}}}{\rho_{\mathrm{ws}}}\right)(n_{\mathrm{ws}}-1)\right], \tag{12}$$

where ρ_{axs} and n_{axs} are, respectively, the density and the refractive index of dry air at standard conditions (15 °C, 101 325 Pa, 0 %rh, 450 ppm of CO_2); ρ_{ws} and n_{ws} are, respectively, the density and the refractive index of pure water vapor at standard conditions (20 °C, 1333 Pa); and ρ_{a} and ρ_{w} are, respectively, the dry-air and water-vapor densities for the environmental conditions in the observation context. All the input variables mentioned are calculated by mathematical models described in [4].

2.2 Contribution of Thermal Effects to Atmospheric Turbulence

The relation between temperature and turbulence can be expressed by a mathematical model of the physical phenomenon according to [2]. In this comprehensive model, the air layers close to the ground are divided in infinitesimal elements of height $\mathrm{d}Z$ and with top and bottom surfaces areas $\mathrm{d}S$. Each of these elements is subjected to the following three vertical forces: (i) the downward force resulting from atmospheric pressure on the top surface, $(P+\mathrm{d}P)\mathrm{d}S$; (ii) the weight of the air element, W, in the downward direction; and (iii) the upward force of the atmospheric pressure on the bottom surface $(P\,\mathrm{d}S)$. The equilibrium condition is given by

$$\frac{\mathrm{d}P}{\mathrm{d}Z} = -g\rho, \tag{13}$$

considering that the weight of the air element corresponds to

$$W = g\rho \mathrm{d}Z\mathrm{d}S, \tag{14}$$

where g is the acceleration of gravity and ρ is the air density.

In a stable thermal scenario, the condition $\mathrm{d}P \geq -g\rho\mathrm{d}Z$ is verified, i.e., the descendent forces (resulting from the weight and pressure on the top surface of the air element) equalize or prevail over the ascendant force (originated by the pressure on the bottom surface of the air element). In this situation, the atmospheric air masses stratify in altitude decreasing density layers and no element vertical movement element occurs.

The opposite condition, $\mathrm{d}P < -g\rho\mathrm{d}Z$, causes an unstable thermal scenario where the air elements within atmospheric layers close to a certain object (for instance, the bridge's foundation in the observation scenario that was studied) are heated by conduction, convection, or radiation, increasing their temperature and, consequently, their pressure and volume, thus causing an air density decrease and ascendant forces to become dominant. In this situation, the air elements tend to move upward, interacting with the above air elements which, in their turn, go downward and start to be heated and, subsequently, also tend to move upward. These upward warm and downward cold air vertical movements are mostly responsible for the atmospheric turbulence phenomenon,[2] where the corresponding dynamic changes in the air refractive index originate an atmospheric scintillation effect on light propagating through the atmosphere.

The boundary condition between a stable and an unstable scenario occurs when the air density vertical gradient becomes null. Since air can be assumed as a perfect gas, the equation of state is

$$\rho = \frac{MP}{RT}, \tag{15}$$

where M is the air molar mass, R is the universal gas constant, and T is the air temperature, which allows writing

$$\frac{\mathrm{d}T}{\mathrm{d}Z} = \frac{T}{P}\frac{\mathrm{d}P}{\mathrm{d}Z}. \tag{16}$$

The substitution of Eq. 13 into Eq. 16 gives an expression for the vertical thermal gradient that is the boundary condition between a stable and an unstable scenario as

$$\frac{\mathrm{d}T}{\mathrm{d}Z} = -\frac{T}{P}g\rho, \tag{17}$$

noticing that, for a stable observation scenario, the condition $\frac{\mathrm{d}T}{\mathrm{d}Z} \geq -\frac{T}{P}g\rho$ is verified. As seen in Eq. 17, the vertical thermal gradient value depends on the air density. Due

[2] Horizontal pressure gradients (wind) can also lightly increase the atmospheric turbulence by contributing to the mixture of different warm or cold air layers. In a radiometric perspective, turbulence can also be caused by partial coherence of the observed light source.

to the high spatial and temporal hygrometric variability in the observation scenario, the density quantity is related to moist air and, therefore, the CIPM-2007 formula [5] can be adopted for the calculation of the moist air density.

In the studied case—long-distance (close to 500 m) optical measurement of suspension bridge displacement—a knowledge of local vertical thermal gradients near cameras or targets can be compared with the critical value obtained from Eq. 17 in order to evaluate the observation stability related to atmospheric turbulence.

Vertical thermal gradients can be obtained by two methods: (i) direct measurements of air temperature at different heights [6]; (ii) meteorological parametric models, based on atmospheric physics theory, which take into account several variables, namely: radiant heat flux density, wind speed, geographic location, altitude, year season, time of day, and ground coverage [7]. A comparative analysis of the two methods mentioned shows that the method performing direct measurements of air temperature is easier to apply since it requires fewer variables than the meteorological approach, with this the reason to use it in this study.

3 Experimental Apparatus

3.1 Introduction

Local air-temperature vertical gradients were measured in the installation region of the optical measurement system in the 25th of April Bridge in Lisbon (see Fig. 2), namely, in the south tower foundation, where the infrared active targets are installed, and in the central section of the bridge's main span, which is the location of the digital camera, rigidly attached to the lower region of the stiffness beam. The length of the line of sight established between the camera and the set of targets is, approximately, 500 m and the corresponding targets/camera height difference is close to 60 m.

The same set of environmental measurements were recorded during *in situ* beam wandering and calibration tests, where a line of sight was established between the

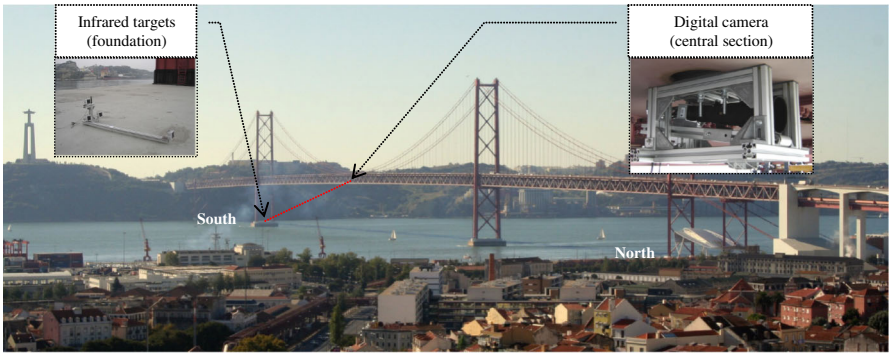

Fig. 2 25th of April Bridge showing the location of the optical displacement measurement system

targets installed in the south tower foundation and the south anchorage where a digital camera was placed.

When compared with the bridge's central section, the two regions (foundation and anchorage) have shown reduced dynamics, allow the installation of the two main optical components in nearly static regions and to establish a line of sight symmetric to the measurement line of sight between the central section and the foundation. Although the wind and topographical conditions are different, the camera remains, approximately, at the same altitude in both geometrical configurations, so the environmental experimental data can be used, in a first approach, to evaluate its influence on the resulting atmospheric scintillation and on the deviations obtained from calibration.

3.2 Measurement Systems and Procedures

The local vertical thermal gradients were determined by direct measurements of air temperature at different heights, using five thermohygrometric sensors vertically distributed in a 2 m rod installed in a tripod, with each sensor protected from direct and indirect sun radiation by a natural ventilated Teflon shield.

The five sensors correspond to Ø15 mm × 100 mm standard industrial sensors (Rotronic Hygromer® IN-1, Pt100 Class A) connected to a data logger (Rotronic HL-NT2) and corresponding docking station (Rotronic HL-DS-U2). Traceability to national primary standards was assured in the measurement range of temperature from 0 °C to 50 °C and from 20 % to 95 % relative humidity, within an instrumental measurement uncertainty of 0.3 °C in temperature and 1.5 % in relative humidity.

Two sets of instrumented rods were prepared for the required field measurements, each one with its own vertical sensor distribution, according to the installation region in the bridge. For the instrumented rod installed in the south tower foundation, the established sensor vertical distances to the foundation top surface were 0.01 m-0.25 m-0.50 m-1.0 m-1.99 m. The same distance values were adopted for the case of the instrumented rod installed in the central section of the bridge's main span, however, relative to the lower surface of the stiffness beam.

After the complete installation of each measurement rod, an acquisition rate of one sample every 60 s was defined for a period of 1 h.

In addition to these measurements, wind-speed measurements were performed simultaneously with the same acquisition rate, aiming to quantify the relation between the thermohygrometric measurements and possible correlations with other quantities. For this purpose, traceable anemometers were installed: (i) on south tower foundation measurement—analog windmill anemometer (Airflow/SN25947) with four measurement ranges ($0.2\,\mathrm{m{\cdot}s^{-1}}$ to $1\,\mathrm{m{\cdot}s^{-1}}$; $1\,\mathrm{m{\cdot}s^{-1}}$ to $2.5\,\mathrm{m{\cdot}s^{-1}}$; $2\,\mathrm{m{\cdot}s^{-1}}$ to $10\,\mathrm{m{\cdot}s^{-1}}$; $10\,\mathrm{m{\cdot}s^{-1}}$ to $25\,\mathrm{m{\cdot}s^{-1}}$) and a division of $0.1\ \mathrm{m{\cdot}s^{-1}}$ for low wind speeds (bellows, $2.5\,\mathrm{m{\cdot}s^{-1}}$) or $1\,\mathrm{m{\cdot}s^{-1}}$ for higher values and (ii) on the central section of the bridge's main span—digital windmill anemometer (Omega / HHF300A) with measurement range between $0.2\ \mathrm{m{\cdot}s^{-1}}$ and $40\ \mathrm{m{\cdot}s^{-1}}$ and a resolution of $0.1\ \mathrm{m{\cdot}s^{-1}}$.

4 Results

4.1 Vertical Thermohygrometric Gradients

The previously described experimental apparatus allowed measuring the main environmental influence quantities (air temperature, relative humidity, and wind speed), in the central section of the bridge's main span and in the south tower foundation for a period of 1 h (from 11:25 to 12:15 in the central section and from 14:50 to 15:50 in the south tower foundation) on June 5, 2013.

From the obtained measurement results, several remarks can be made:

(i) central section of the bridge's main span:
   (a) the air temperature had an average value of 18.1 °C with a minimum of 17.8 °C and a maximum of 18.4 °C, with the higher values obtained for the region closer to the lower surface of the stiffness beam (due to radiation heat transmission from the bridge to the air and lower convection effect by reduced wind speed);
   (b) the relative humidity, for the same observation, had an average value of 66 %, and changed between a minimum of 64 % and a maximum of 69 %, noticing that its temporal evolution was opposite to the air-temperature evolution; the relative humidity is considered to stabilize at the same period of stabilization of temperature, at the end of the record;
   (c) the wind speed had an average value of 2.1 $m \cdot s^{-1}$, having a minimum of 1.0 $m \cdot s^{-1}$ and a maximum of 2.9 $m \cdot s^{-1}$, showing a stable behavior in the first part (until 12:10); from this point forward, the wind speed decreased for lower values and the corresponding convection effect begins to influence the stabilization of the thermohygrometric profiles; during the observation time period, the wind direction remained approximately constant in the southwest/west direction; measurements refer to the lower surface of the stiffness beam (where the camera will be installed) and not to the lateral wind incident surface, where higher wind-speed values were observed (typically, two times higher).

(ii) south tower foundation:
   (a) the air temperature had an average value of 24.8 °C, with a minimum of 21.4 °C and a maximum of 29.4 °C; due to the radiation heat transmission from the foundation top surface (heated by incident solar radiation), the highest air-temperature values were recorded for the vertical position closest to the ground (0.01 m) noticing that, for the remaining vertical positions, air-temperature differences between consecutive positions showed a reduced magnitude when compared with air-temperature differences for the 0.01 m and 0.25 m positions;
   (b) the relative humidity, for the same observation, had an average value of 45 %, with a minimum of 34 % and a maximum of 55 %; as observed for the central section of the bridge's main span, again as expected, the hygrometric temporal evolution was opposite to the air-temperature evolution;
   (c) an average wind-speed value of 1.4 $m \cdot s^{-1}$ was recorded, with minimum values (close to zero) obtained in the first part of the observation period (from 14:50 to 15:32) and a maximum of 4.5 $m \cdot s^{-1}$ obtained in the second part, near the end of the record, following a significant increase of the wind speed; this difference

can be justified by the variation of the wind direction from west to northwest (around 15:32) and the fact that the anemometer was aligned with the bridge's tower in the west direction, thus being more exposed to other wind directions, namely, to the northwesterly wind; this change in wind direction can be viewed in the thermohygrometric records since the relative difference between consecutive vertical measurement positions decreased, becoming almost null due to the wind convective effect, with the exception of the vertical position closest to the surface, where the radiation effect prevailed;

(iii) a comparative analysis between the two observation regions shows that the lower region of the bridge's main span has a reduced spatial and temporal thermal variability when compared with the tower foundation due to different exposure conditions noticing that, during daytime, the lower surface of the stiffness beam is protected from direct sun exposure and wind action; in both regions and considering all the studied vertical positions, the air temperature and relative humidity showed a similar response to environmental changes.

Based on the measurement estimates, it was possible to evaluate the spatial and temporal distribution of the refractive-index estimates at the central section of the bridge's main span and at the south tower foundation. The following remarks are based on the obtained results:

(i) central section of the bridge's main span:
  (a) the analysis of the vertical thermal distribution beneath the lower surface of the stiffness beam found a typical linear decrease of the temperature in an interval of height between 61 m and 62 m, being possible to establish a constant vertical thermal gradient with small nonlinear effects that can be observed close to the surface of the stiffness beam (mainly due to radiation and convective heat transmission phenomena); in the height interval, from 60 m up to 61 m, a small air-temperature increase was observed, being related to the presence of the movable platform where the instrumented rod was installed underneath the stiffness beam;
  (b) regarding the relative humidity, the analysis of the data shows the stability of the quantity, allowing to assume a constant level of humidity in the vertical position range of 60 m up to 62 m during the same observation time; therefore, a null hygrometric vertical gradient can be assumed to represent this region;
  (c) the calculated spatial and temporal evolution of the refractive index near the lower region of the stiffness beam reflects a significant influence of the thermal behavior described above (see item a.), having a linear increase (constant vertical gradient of, approximately, $-10^{-7}\,\mathrm{m}^{-1}$) for the height decrease (range of 61 m to 62 m); in the remaining height interval, a small decrease of the refractive index was found, as expected, due to the thermal influence of the movable platform.

(ii) south tower foundation:
  (a) the study of the conditions near the foundation top surface shows a nonlinear relationship between the air temperature and the height, showing a temperature decrease with altitude increase according to a power-law parametric model $t\,(Z) = aZ^b$(a reasonable adjustment to the experimental data, namely, for

Table 1 Power-law parametric modeling, $t\,(Z) = aZ^b$, of the vertical air-temperature distribution in the south tower foundation, between 0.01 m and 1.99 m (2013-06-05)

Time	a	b	Maximum residual deviation (°C)
15:00	$26.360\,^{\circ}\mathrm{C}\cdot\mathrm{m}^{0.0226}$	-2.26×10^{-2}	0.36
15:20	$24.087\,^{\circ}\mathrm{C}\cdot\mathrm{m}^{0.0217}$	-2.17×10^{-2}	0.07
15:30	$23.131\,^{\circ}\mathrm{C}\cdot\mathrm{m}^{0.0194}$	-1.94×10^{-2}	0.07
15:40	$22.043\,^{\circ}\mathrm{C}\cdot\mathrm{m}^{0.0162}$	-1.62×10^{-2}	0.09
15:50	$21.491\,^{\circ}\mathrm{C}\cdot\mathrm{m}^{0.0106}$	-1.06×10^{-2}	0.28

Table 2 Power-law parametric modeling, $hr\,(Z) = aZ^b$, of the relative-humidity vertical distribution in the south tower foundation, between 0.01 m and 1.99 m (2013-06-05)

Time	a	b	Maximum residual (%)
15:00	$39.336\,\%\cdot\mathrm{m}^{-0.0333}$	3.33×10^{-2}	1.1
15:20	$46.867\,\%\cdot\mathrm{m}^{-0.0304}$	3.04×10^{-2}	0.7
15:30	$49.674\,\%\cdot\mathrm{m}^{-0.0265}$	2.65×10^{-2}	0.7
15:40	$54.262\,\%\cdot\mathrm{m}^{-0.0221}$	2.21×10^{-2}	0.6
15:50	$52.805\,\%\cdot\mathrm{m}^{-0.0148}$	1.48×10^{-2}	0.7

Table 3 Power-law parametric modeling, $n(Z) = aZ^b$, of the refractive-index vertical evolution in the south tower foundation, between 0.01 m and 1.99 m (2013-06-05)

Time	a	b	Maximum residual
15:00	$1.000\,263\,614\,\mathrm{m}^{-5.49\times10^{-7}}$	5.49×10^{-7}	3.15×10^{-7}
15:20	$1.000\,265\,619\,\mathrm{m}^{-4.88\times10^{-7}}$	4.88×10^{-7}	0.67×10^{-7}
15:30	$1.000\,266\,479\,\mathrm{m}^{-4.21\times10^{-7}}$	4.21×10^{-7}	0.46×10^{-7}
15:40	$1.000\,267\,455\,\mathrm{m}^{-3.35\times10^{-7}}$	3.35×10^{-7}	0.95×10^{-7}
15:50	$1.000\,267\,992\,\mathrm{m}^{-2.13\times10^{-7}}$	2.13×10^{-7}	2.59×10^{-7}

the observation time period between 15:20 and 15:40—see Table 1), giving a nonlinear vertical thermal gradient, $\frac{\mathrm{d}t}{\mathrm{d}Z} = abZ^{b-1}$;

(b) the vertical spatial distribution of the relative humidity also shows a nonlinear relation relative to the height from the foundation top surface, being opposite to the air-temperature distribution, i.e., a height increase corresponds to a relative-humidity increase; again, the power-law parametric model $hr\,(Z) = aZ^b$ allows a reasonable adjustment to the experimental data, namely, for the observation time period between 15:20 and 15:50, as shown in Table 2;

(c) as a consequence of the nonlinear thermohygrometric vertical distribution mentioned, the refractive index of humid air in the south tower foundation also has a nonlinear relation, increasing with the height from the top surface, especially in the height range between 0.01 m and 0.50 m; Table 3 presents the estimates of the model parameters for the adopted power law of the refraction index, $n\,(Z) = aZ^b$, for which the vertical gradient corresponds to $\frac{\mathrm{d}n}{\mathrm{d}Z} = abZ^{b-1}$.

(iii) the comparative analysis of the non-simultaneous measurement records (with a 2.5 h gap between records related to both studied regions) allows the conclusion that the south tower foundation is characterized by higher and nonlinear vertical

thermal gradients when compared with the lower region of the bridge's stiffness beam, which is not as exposed to direct solar radiation during daytime (due to the shadow effect of the stiffness beam); this fact is reflected on the observed vertical hygrometric gradient and on the corresponding refractive index which also shows a nonlinear relation near the foundation; considering the magnitude of the refractive-index vertical variations in the lower surface of the stiffness beam (61 m to 62 m range), it is possible to consider reasonable, in this case, to adopt a linear behavior.

4.2 Turbulence Analysis

The study concerning turbulence phenomenon (for the same time interval of Sect. 4.1 results) was supported on the observation of the conditions near the top surface of the south tower foundation and revealed the existence of high thermal gradients leading to atmospheric scintillation. A comparison of the experimental vertical thermal gradients (obtained from the power-law model described in the previous section) and the corresponding limit value for the stable/unstable theoretical boundary (see Eq. 17 in Sect. 2.2) can be made for the south tower region, as shown in Table 4.

This table shows that unstable observation conditions due to turbulence were identified for all the studied positions since the experimental vertical thermal gradient values were lower than the calculated limit gradient, namely, for heights below 0.25 m.

Table 4 Experimental and boundary limit vertical thermal gradients in the south tower foundation (2013-06-05)

Height:	0.01 m		0.25 m		0.50 m	
Time (hh:mm)	$\left(\frac{dt}{dZ}\right)_{exp}$ (°C·m^{-1})	$\left(\frac{dt}{dZ}\right)_{lim}$ (°C·m^{-1})	$\left(\frac{dt}{dZ}\right)_{exp}$ (°C·m^{-1})	$\left(\frac{dt}{dZ}\right)_{lim}$ (°C·m^{-1})	$\left(\frac{dt}{dZ}\right)_{exp}$ (°C·m^{-1})	$\left(\frac{dt}{dZ}\right)_{lim}$ (°C·m^{-1})
15:00	−66.11	−0.0033	−2.46	−0.0030	−1.21	−0.0026
15:20	−57.76	−0.0031	−2.15	−0.0028	−1.06	−0.0025
15:30	−49.07	−0.0030	−1.84	−0.0028	−0.91	−0.0025
15:40	−38.48	−0.0030	−1.46	−0.0028	−0.72	−0.0025
15:50	−23.92	−0.0029	−0.92	−0.0027	−0.46	−0.0025
Height:	1.00m		1.99m			
Time (hh:mm)	$\left(\frac{dt}{dZ}\right)_{exp}$ (°C·m^{-1})	$\left(\frac{dt}{dZ}\right)_{lim}$ (°C·m^{-1})	$\left(\frac{dt}{dZ}\right)_{exp}$ (°C·m^{-1})	$\left(\frac{dt}{dZ}\right)_{lim}$ (°C·m^{-1})		
15:00	−0.60	−0.0027	−0.29	−0.0026		
15:20	−0.52	−0.0026	−0.26	−0.0025		
15:30	−0.45	−0.0026	−0.22	−0.0025		
15:40	−0.36	−0.0025	−0.18	−0.0025		
15:50	−0.23	−0.0025	−0.11	−0.0025		

Table 5 Experimental and boundary limit vertical thermal gradients in the lower region of the stiffness beam (2013-06-05)

Time (hh:mm)	$\left(\frac{dt}{dZ}\right)_{exp}$ (°C·m^{-1})	$\left(\frac{dt}{dZ}\right)_{lim}$ (°C·m^{-1})
11:25	0.11	−0.0021
11:45	0.13	−0.0021
11:55	0.12	−0.0021
12:05	0.11	−0.0021
12:25	0.16	−0.0021

As expected, the difference between the experimental and the limit values tends to decrease with the height increase. However, even for the vertical position of 1.99 m, unstable observation conditions are obtained.

The same type of analysis can be performed for the lower region of the stiffness beam using the recorded air-temperature values. Due to the radiant influence of the movable platform (see previous section), the temperature values referring to the vertical position of 60 m were not considered in the determination of the experimental vertical thermal gradient by a linear regression. The obtained results are presented in Table 5.

The comparison of vertical thermal gradients in the lower region of the stiffness beam shows that stable observation conditions were established in it (from 61 m up to 62 m), as the experimental estimate of the vertical thermal gradient is above the limit of the vertical thermal gradient. This means that, again, an opposition is found when conditions are observed for the south tower foundation, showing that this initial region of the optical trajectory (where the set of active targets is installed) can be subjected to turbulence able to influence the digital images of the targets to be recorded.

4.3 Vertical Refraction Angle and Deviation

Simultaneous measurements of the air temperature, relative humidity, and wind speed were performed in the south tower foundation and in the lower region of the stiffness beam close to the south anchorage on July 9, 2013, during the performance of beam wandering and calibration testing with the optical measurement system, allowing evaluation of the refractive index at different vertical heights (respectively, 0.5 m and 61 m). The environmental records obtained are presented in Figs. 3, 4, and 5 while Fig. 6 shows the corresponding refractive index calculated for a near-infrared radiation wavelength of 875 nm. The atmospheric pressure remained stable during the experimental records, namely, in the south tower foundation (1015 hPa) and in the south anchorage (1008 hPa).

As shown in Fig. 3, the thermal measurements obtained simultaneously showed an air-temperature difference between the foundation region and the lower region of the stiffness varying from a minimum value of, approximately, 1.1 °C, to a maximum difference close to 7.8 °C. It is also noteworthy that, during the observation, the air temperature near the stiffness beam remained stable while in the foundation, an air-temperature increase was measured at around 12:20 until 12:45. From this point forward, the air temperature started to decrease, mainly, due to the tower shadow effect on the foundation top surface.

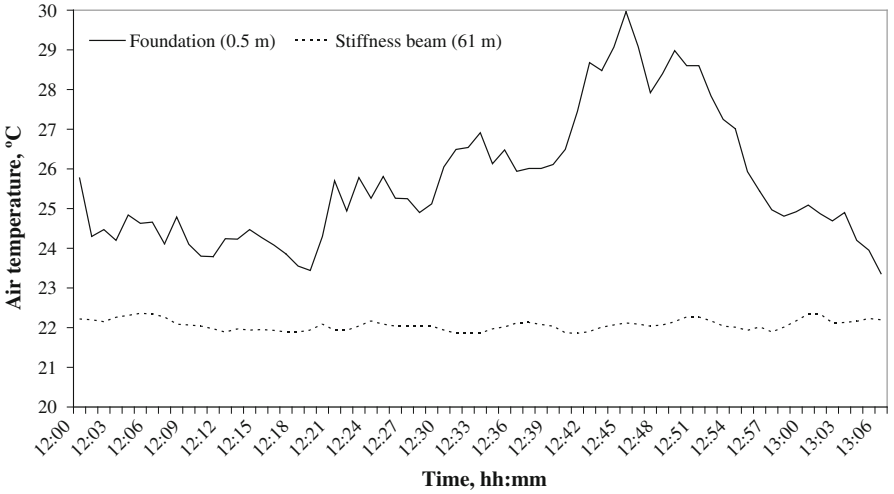

Fig. 3 Air-temperature temporal record (2013-07-09)

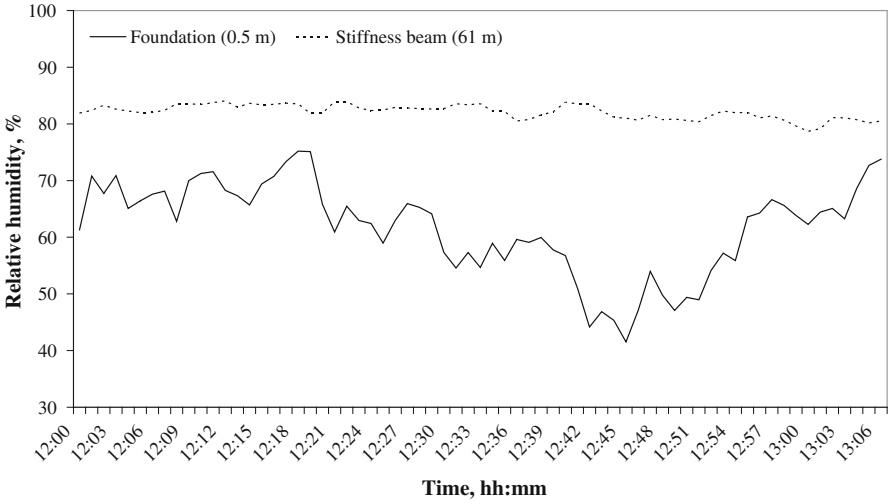

Fig. 4 Relative-humidity temporal record (2013-07-09)

The hygrometric records (see Fig. 4) for the same period also showed that the stiffness beam region had a more stable behavior (with a relative humidity slightly above 80 %) when compared with the hygrometric condition near the foundation, where lower relative humidity values were obtained. The relative-humidity difference between the two studied regions varied between 7 % and 40 %.

For the same period, higher wind-speed values were recorded in the south tower foundation (with an average wind speed of 5.4 $m \cdot s^{-1}$) when compared to the stiffness beam record (where the average wind speed was 1.3 $m \cdot s^{-1}$) as shown in Fig. 5, considering a northwest wind direction in both regions.

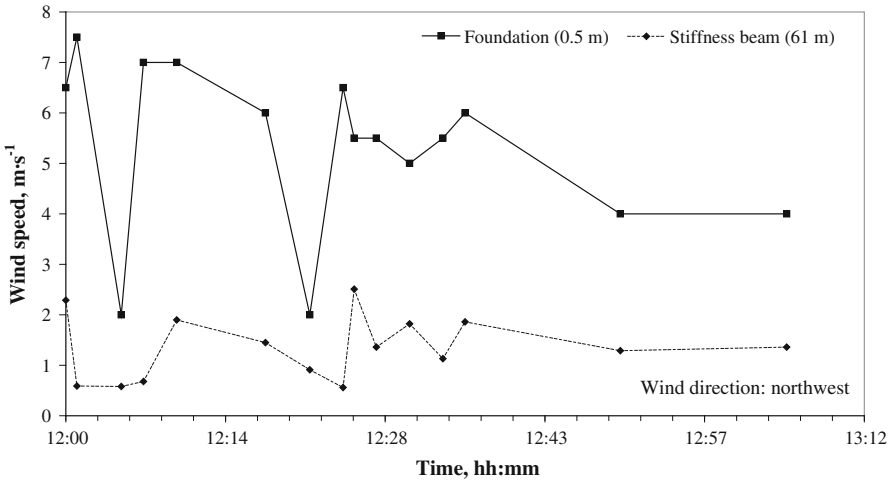

Fig. 5 Wind-speed temporal record (2013-07-09)

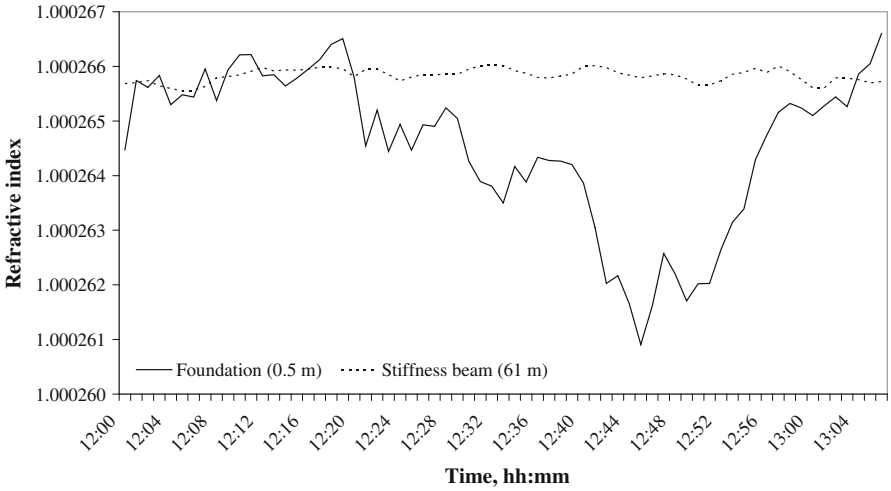

Fig. 6 Calculated refractive-index temporal evolution (2013-07-09)

The temporal evolution of the corresponding refractive index in both observation regions shows minor differences between them in a first period (12:00 to 12:20), even considering air-temperature and relative-humidity differences close to 2 °C and 10 %, respectively. This fact can be justified by the barometric difference between the foundation (where measurements were performed in a vertical position of 0.5 m) and the lower region of the stiffness beam (in a nominal vertical position of 61 m). In the following period (after 12:20), the air temperature increased in the foundation starting to be reflected in the refractive index and a maximum difference of, around, 5×10^{-6} between the two studied regions was reached at 12:45, returning afterwards to the initial situation.

Table 6 Vertical refraction angles and deviations obtained by the constant refractive-index gradient approach (2013-07-09)

Time:	12:15						
Quantities	X	Z	ε	t	rh	p_{atm}	n
Foundation	0 m	0.5 m	105.279 mrad	24.27 °C	69.39 %	1015 hPa	1.000 265 785
Beam	582 m	61 m		21.95 °C	83.34 %	1008 hPa	1.000 265 930
n_0	1.000 265 784						
α	2.4×10^{-9} m^{-1}						
δ	−0.6 μrad						
ΔZ	−0.4 mm						
Time:	12:45						
Quantities	X	Z	ε	t	rh	p_{atm}	n
Foundation	0 m	0.5 m	105.279 mrad	29.96 °C	41.53 %	1015 hPa	1.000 260 905
Beam	582 m	61 m		22.12 °C	81.01 %	1008 hPa	1.000 265 792
n_0	1.000 260 866						
α	79.5×10^{-9} m^{-1}						
δ	−23.4 μrad						
ΔZ	−13.6 mm						

Based on the analysis presented, it is appropriate to assume that a constant refractive-index gradient method (described in Sect. 2) can be used as a first linear approach, in order to quantify the vertical refraction angle and the deviation for two situations of interest: a minor refractive-index difference, for example, considering the observation conditions recorded at 12:15; and a major refractive-index difference, taking into account the observational conditions at 12:45. The main input and output quantities estimates are presented in Table 6.

The analysis of the data in the previous table reveals a significant difference between the vertical refraction angles and the estimates of deviations obtained for the two studied moments of time. In the first moment (at 12:15), the vertical refractive-index gradient has a reduced magnitude (2.4×10^{-9} m^{-1}) leading to a reduced vertical refraction angle and, consequently, a minor vertical deviation by refraction (−0.4 mm). In the second moment (at 12:45), the higher magnitude of the observed vertical thermal gradient between the foundation and the stiffness beam was reflected in a higher vertical refractive-index gradient (79.5×10^{-9} m^{-1}) when compared with the previous one. The obtained vertical refraction angle and the deviation by refraction cannot be neglected in the accuracy evaluation of the optical measurement system.

Complementary to the constant gradient approach applied, the vertical refraction angles and deviations mentioned can also be determined by the geodesic approach (see Sect. 2), using the same vertical refractive-index gradients values for the two time moments analyzed in particular. The obtained results are presented in Table 7.

The previous table shows minor differences in the results obtained by both approaches, considering the absence of nonlinear effects on the vertical refractive-

Table 7 Comparison of vertical refraction angles and deviations obtained by different approaches (2013-07-09)

Time:	12:15		12:45	
Quantity	δ (μrad)	ΔZ (mm)	δ (μrad)	ΔZ (mm)
Constant gradient approach	−0.6	−0.4	−23.4	−13.6
Geodesic approach	−0.7	−0.4	−23.1	−13.5

index gradient. However, the results obtained for the south tower foundation (see Sect. 4.1) shows that, in certain observation scenarios, a significant nonlinear thermal environment may be observed close to its top surface, requiring the quantification of these effects on the vertical refraction deviations. Since the geodesic approach allows consideration of the existence of nonlinear effects in the initial region of the light trajectory, it was used for the estimation of vertical refraction deviations based on the nonlinear parametric models obtained for the vertical refractive index presented in Sect. 4.1 (see Table 3). These models were used to evaluate the refractive index and its gradient in the initial and middle positions of the light trajectory.

The previous figures emphasize the importance of the refraction phenomenon in the optical system's accuracy considering that significant vertical refraction angles and deviations (above 12 μrad and −7 mm, respectively) can be expected in adverse observation conditions, such as the ones recorded for the south tower foundation. In the studied observation time period, for the placement of the targets in the vertical position of 0.5 m from the foundation surface, the vertical refraction deviations change from −65 mm (at 15:00), decreasing to −25 mm (at 15:50). The nonlinear air-temperature vertical distribution makes the vertical refraction deviation strongly dependent on the target's height relative to the foundation surface. To illustrate this situation, considering as an example a target height increase of the vertical position from 0.5 m to 1.0 m, the magnitude reduction of the vertical refraction deviations observed would reduce to nearly 50 % of the initial value.

5 Conclusions

This study has allowed improvement of the knowledge about the thermal influence on long-distance optical measurements of suspension bridge displacement. In a global perspective, the studied observation scenario (the 25th of April Bridge) showed a high spatial and temporal thermal variability related to the season of the year (summer), the absence of cloud coverage, shadow effects, and the time of day (in the afternoon period) during which the experiments were performed.

In a local perspective, the two studied regions—the south tower foundation and the lower region of the bridge's stiffness beam—showed different thermal behavior, with the tower foundation more exposed to incident solar radiation and convection effects than the lower surface of the stiffness beam. In particular, the tower foundation region has shown a considerable nonlinear performance based on the relation between thermohygrometric quantities and height from its top surface, with it reasonable to

describe it by a power-law vertical evolution. On the other side, the lower region of the stiffness beam showed a linear vertical distribution of the air temperature and nearly null hygrometric vertical gradients. These thermal behaviors influenced the corresponding vertical distribution of the refractive index in both studied regions, following a nonlinear power law in the tower foundation and a linear vertical evolution near the lower surface of the stiffness beam.

The same thermal relations were used for turbulence analysis of the studied regions, identifying an unstable condition for all the vertical positions in the south tower foundation and a stable condition in the lower region of the stiffness beam, making the foundation region a major source of concern when dealing with the turbulence phenomenon since active infrared targets are intended to be installed there.

The simultaneous environmental measurements performed during beam wandering and calibration tests of the optical system allowed observation of a high thermal spatial difference between the stiffness beam and the tower foundation (with a height difference close to 60 m) which is reflected on the corresponding refractive index. A significant change in the refractive-index vertical distribution is noticed for an air-temperature difference above 2 °C.

The constant refractive-index gradient and the geodesic approaches were used to estimate the vertical refraction angle and target deviation for two distinct thermal situations, lower than and above the mentioned 2 °C air-temperature difference between the foundation and the stiffness beam. Both the approaches caused similar results, showing minor vertical refraction angles and target deviations (0.6 μrad and −0.4 mm, respectively) for the lower air-temperature difference (around 2 °C) and major values (23 μrad and −14 mm, respectively) for the higher air-temperature difference (close to 8 °C).

The geodesic approach allowed consideration of the nonlinear thermal behavior observed in the south tower foundation. The obtained results showed a significant increase in the magnitude of the vertical refraction angles and deviations. Considering that the optical system installed in the 25th of April Bridge has a instantaneous-field-of-view (IFOV) close to 12 μrad and the estimated vertical refraction angles obtained for the south tower foundation are all above this value, valid even for the higher vertical target positions, the optical system will be sensitive to changes in the light ray propagation direction by the vertical refraction effect.

Based on the performed work, a measurement uncertainty evaluation of the vertical refraction correction is now possible since major uncertainty sources related to the vertical refractive-index gradient, namely, the instrumental thermohygrometric uncertainty and the residues produced by the power-law modeling, are now known.

Due to the complex nature of the described mathematical models, the Monte Carlo method will be use to perform the propagation of the mentioned input uncertainties (in addition with other uncertainty sources, namely, measurement geometrical configuration and the moist air refractivity) to the refraction correction, allowing determination if the achieved accuracy is suitable for the studied measurement problem and, in its turn, combined with the remaining measurement uncertainties related to three-dimensional bridge displacement through the use of optical systems.

Since the optical measurement system is used for continuous displacement monitoring, additional experimental work is required in order to have an extended knowledge

about the environmental conditions in different seasons of the year (namely, during winter season) and time of day and night. This collected data will be useful for setting operational parameters of the optical measurement system.

Acknowledgments The authors gratefully acknowledge the company EP—Estradas de Portugal, S.A. who authorized and supported the experimental work performed on the 25th of April Bridge and to the Colleagues of the Scientific Instrumentation Centre of LNEC that provided experimental assemblies and technical support. The anemometers used in the experimental work were gently provided by Dr. Marques da Silva from LNEC's Aerodynamic Sector. The author L. Lages Martins also acknowledges the award of a joint doctoral scholarship from the FCT—Fundação para a Ciência e a Tecnologia, I.P. and LNEC—Laboratório Nacional de Engenharia Civil, I.P.

References

1. Y. Qiao, Acta Opt. Sin. **4**, 984 (1984)
2. J. Casaca, *Atmospheric Refraction in Applied Geodesy* (LNEC, Lisbon, 2004)
3. M. Aikawa, T. Hiraki, Meteorol. Atmos. Phys. **104**, 95 (2009)
4. P.E. Ciddor, Appl. Opt. **35**, 1566 (1996)
5. A. Picard, R.S. Davis, M. Gläser, K. Fujii, Metrologia **45**, 149 (2008)
6. G.A. Kharaghani, Propagation on Refraction Errors in Trigonometric Height Traversing and Geodetic Levelling, M.Sc. Thesis, Technical Report No. 132, University of New Brunswick, 1987, pp. 6–19
7. E.K. Webb, *Temperature and Humidity Structure in the Lower Atmosphere in Geodetic Refraction* (Springer, Berlin, 1984)